Design and Synthesis of *de Novo* Cytochromes *c*†

Manabu Ishida,‡,§ Naoshi Dohmae,|| Yoshitsugu Shiro,‡,§ Tadatake Oku,⊥ Tetsutaro Iizuka,‡ and Yasuhiro Isogai*,‡,||

RIKEN Harima Institute/SPring-8, Mikazuki-cho, Sayo, Hyogo 679-5143, Japan, Department of Life Science, Faculty of Science, Himeji Institute of Technology, Ako-gun, Hyogo 678-1297, Japan, Biomolecular Characterization Team, RIKEN, Wako, Saitama 351-0198, Japan, and Department of Biological Chemistry, College of Bioresource Sciences, Nihon University, 1866 Kameino, Fujisawa, Kanagawa 252-8510, Japan

Received March 8, 2004; Revised Manuscript Received May 31, 2004

ABSTRACT: Natural *c*-type cytochromes are characterized by the consensus Cys-X-X-Cys-His heme-binding motif (where X is any amino acid) by which the heme is covalently attached to protein by the addition of the sulfhydryl groups of two cysteine residues to the vinyl groups of the heme. In this work, the consensus sequence was used for the heme-binding site of a designed four-helix bundle, and the apoproteins with either a histidine residue or a methionine residue positioned at the sixth coordination site were synthesized and reacted with iron protoporphyrin IX (protoheme) under mild reducing conditions *in vitro*. These polypeptides bound one heme per helix−loop−helix monomer via a single thioether bond and formed four-helix bundle dimers in the holo forms as designed. They exhibited visible absorption spectra characteristic of *c*-type cytochromes, in which the absorption bands shifted to lower wavelengths in comparison with the *b*-type heme binding intermediates of the same proteins. Unexpectedly, the designed cytochromes *c* with bis-His-coordinated heme iron exhibited oxidation−reduction potentials similar to those of their *b*-type intermediates, which have no thioether bond. Furthermore, the cytochrome *c* with His and Met residues as the axial ligands exhibited redox potentials increased by only 15−30 mV in comparison with the cytochrome with the bis-His coordination. These results indicate that highly positive redox potentials of natural cytochromes *c* are not only due to the heme covalent structure, including the Met ligation, but also due to noncovalent and hydrophobic environments surrounding the heme. The covalent attachment of heme to the polypeptide in natural cytochromes *c* may contribute to their higher redox potentials by reducing the thermodynamic stability of the oxidized forms relatively against that of the reduced forms without the loss of heme.

De novo protein design is an important approach to elucidating the principles of protein structure and function (*1*−*5*). In this respect, several artificial heme proteins have been designed and synthesized as the analogues for cytochromes (*6*−*9*) and myoglobins (*10*, *11*). Four-helix bundle motifs were frequently used to realize a *b*-type cytochrome in the artificial systems. In these designed four-helix bundles, two histidine residues were positioned at the opposite sites across the hydrophobic interface between two helices and the heme was associated with the protein in the bis-His six-coordinated state of the iron. These artificial heme proteins exhibited UV−visible absorption spectra similar to those of natural cytochrome *b* in the ferric and ferrous forms and underwent one-electron oxidation−reduction reactions with midpoint potentials around −200 mV versus SHE, which are in the lower range of the potentials exhibited by natural *b*-type cytochromes. The affinities of these artificial proteins for heme are in the dissociation constant (K_d) range from nanomolar to several micromolar and are much lower than those of natural cytochromes. The effects of the affinity for heme on the redox properties and the rational strategy for sequence selection for generating the native-like affinities have not yet been clarified.

Natural *c*-type cytochromes have essential roles in living cells as electron carriers in respiration and photosynthesis, enzymes, and signal transducers and are characterized by the covalent attachment of heme to protein (*12*−*14*). Usually, the heme of cytochrome *c*, in contrast with that of cytochrome *b*, is associated with the protein via two thioether bonds formed by the addition of the sulfhydryl groups of two cysteine residues to the vinyl groups of the heme at the consensus Cys-X-X-Cys-His heme *c*-binding motif, where X is any amino acid. Furthermore, the two axial ligands of the heme iron in cytochrome *c* are methionine and histidine, whereas those in cytochrome *b* are both histidine residues except for that in *Escherichia coli* cytochrome b_{562}. Thus, the higher redox potentials of cytochromes *c* in comparison with those of cytochrome *b* can be attributed to these differences in the heme linkages between the cytochromes as mentioned above. There has been controversy regarding the reaction mechanisms, both spontaneous and enzymatic, by which the covalent bonds are formed between heme and apocytochromes *c*. In living cells, however, the thioether

† This work was supported by the Bioarchitect Research Program of RIKEN and by Grants-in-Aid for Scientific Research from the Ministry of Education, Science, Culture, and Sports of Japan.

* To whom correspondence should be addressed: Biophysical Chemistry Laboratory (Wako Branch), Room 101, Main Research Building, RIKEN, Hirosawa 2-1, Wako, Saitama 351-0198, Japan. Phone: 81-48-467-4583. Fax: 81-48-467-9649. E-mail: yisogai@riken.jp.

‡ RIKEN Harima Institute/SPring-8.

§ Himeji Institute of Technology.

|| RIKEN.

⊥ Nihon University.

10.1021/bi049546e CCC: $27.50
Published on Web 07/08/2004

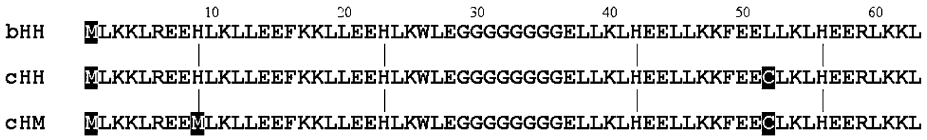

FIGURE 1: Amino acid sequences of the synthesized artificial cytochromes. The outlined codes are the residues different from those of the prototype helix−loop−helix polypeptide (α-*l*-α) designed by Gibney *et al*. (*8*). The vertical lines between the sequences denote the positions assumed to be the heme axial ligands. His-23 and His-42 of these polypeptides correspond to the 10, 10′ site of the prototype (see refs *6* and *8*) and form heme *b*-binding sites near the loop. His-9 (Met-9) and His-54 correspond to the 24, 24′ site of the prototype, and those of cHH and cHM form the heme *c*-binding sites with Cys-52.

bonds seem to be formed with the aid of an enzymatic system for the maturation of cytochrome *c*. Thus, the expression and engineering of native cytochromes *c* (*15*−*18*) and mutational conversion of native *b*-type cytochromes to *c*-type cytochromes (*19*, *20*) were conducted using recombinant *E. coli* either by the *in situ* maturation system or by co-expression of the cytochrome *c* maturation (*ccm*) gene cluster or the heme lyase gene. Recently, Daltrop *et al*. reported that the thioether bonds in a natural cytochrome *c* spontaneously form *in vitro* under mild reducing conditions via a *b*-type heme-binding intermediate in the absence of any biogenesis apparatus (*21*, *22*). In the work presented here, we have adopted a designed four-helix bundle framework with a simplified amino acid sequence (*6*, *8*) for binding heme *c* and synthesized artificial cytochromes *c* by the *in vitro* formation of thioether bonds between heme and the polypeptide. The structural and functional properties were investigated and compared with those of natural cytochromes, their variants, and designed cytochromes *b* to gain insight into the strategy for realizing native-like functional properties in the designed proteins.

MATERIALS AND METHODS

Sequence Design. An amino acid sequence (α-*l*-α) designed by Gibney *et al*. (*8*) to form a heme-binding four-helix bundle ([α-*l*-α]$_2$) was used and modified for binding heme *c* as shown in Figure 1. In our prototype polypeptide bHH (*b*-type bis-His ligation), methionine was added to the N-terminus of α-*l*-α to initiate the protein expression in *E. coli* cells. The binding site for the *c*-type heme was constructed by the replacement of Leu-52 with Cys at the site followed by His-56, which was originally positioned for binding heme *b* on the C-terminal side of the second helix in the helix−loop−helix monomer, to give the sequence CLKLH in the polypeptide cHH (*c*-type bis-His ligation). In the polypeptide cHM (*c*-type His/Met ligation), His-9 was further replaced with Met (Figure 1). See the Discussion for other designed sequences that have been synthesized.

DNA Construction. The artificial gene encoding the prototype polypeptide bHH with the optimal codons of *E. coli* (*23*) was generated by the polymerase chain reaction (PCR) with *Pyrobest* DNA polymerase (Takara Bio Inc.) from three synthetic oligonucleotides: 5′-GGGCATATGCTGAAGAAACTACGCGAAGAACATTTGAAGCTCCTAGAAGAGTTCAAAAAGTTACTCGAAGAGCACTTA-3′ containing the *Nde*I restriction site near the 5′ end, 5′-CTCGAAGAGCACTTAAAATGGCTGGAAGGCGGGGGAGGTGGCGGAGGTGGGGAACTGCTTAAGCTCCACGAGGAATTG-3′, and 5′-GGGAAGCTTACAGCTTTTTCAAACGCTCCTCATGCAGTTTCAGTAATTCCTCGAATTTTTTCAGCAATTCCTCGTGGAG-3′ containing the *Hin*dIII restriction site near the 5′ end. The resulting 205 bp fragment was digested with *Nde*I and *Hin*dIII (Takara Bio Inc.) and cloned into a pRSET-C vector (Invitrogen) using T4 DNA ligase (Takara Bio Inc.) to yield pbHH. The artificial genes encoding *c*-type *de novo* cytochromes were constructed by PCR using pbHH as the template. For example, the gene encoding polypeptide cHM[1] was constructed from pbHH and the two primer DNAs: 5′-GGAGATATACATATGCTGAAGAAACTACGCGAAGAAATGTTGAAGCTCCTAGAAGAG-3′ encoding Met-9 in place of His-9 of the bHH sequence for the sixth coordination ligand and 5′-GCCGGATCAAGCTTACAGCTTTTTCAAACGCTCCTCATGCAGTTTCAGGCATTCCTCGAATTTTTTCAG-3′ encoding Cys-52 in place of Leu-52 of the bHH sequence for the *c*-type heme-binding motif. The resulting fragment was digested with *Nde*I and *Hin*dIII and was cloned into pRSET-C to give pcHM. Other artificial genes were constructed by similar procedures. All the synthetic oligonucleotides were purchased from QIAGEN Inc.

Protein Expression and Purification. An artificial gene in pRSET-C was transformed into *E. coli* strain BL21(DE3) and expressed in 2×YT medium supplemented with 100 mg/L ampicillin under the control of the T7 promoter using isopropyl 1-thio-β-D-galactopyranoside (IPTG). Cells were harvested by centrifugation, washed with TE buffer containing 10 mM Tris-HCl (pH 8.0) and 1 mM ethylenediaminetetraacetic acid (EDTA), and lysed by sonication in TE buffer supplemented with 0.3% (v/v) 2-mercaptoethanol. After addition of polyethyleneimine (PEI) to approximately 0.6%, the insoluble fractions were removed by centrifugation. The supernatants were collected and dialyzed against 0.05% trifluoroacetic acid (TFA) overnight at 4 °C. After removal of the insoluble fractions by centrifugation, the supernatant was concentrated to an appropriate concentration using an AMICON YM-3 ultrafiltration membrane (Millipore). The concentrated solution was centrifuged, and the supernatant was applied onto a C4 reverse-phase preparative HPLC column (Vydac 214TP1022). Apo-cHH and apo-cHM polypeptides were eluted with a gradients 32 to 52% and 36 to 56% acetonitrile, respectively, in the presence of 0.05% TFA with a Hitachi L-6200 HPLC system. The peak fractions containing the designed proteins were collected, evaporated, and lyophilized. The samples were dissolved in water and dialyzed against an appropriate buffer solution. Concentrations of apo-designed cytochromes were determined spectrophotometrically using an ϵ_{280} of 5.8 mM^{-1} cm^{-1} at pH 8, which was estimated from the protein sequence.

[1] Abbreviations: CD, circular dichroism; cHH and cHM, *c*-type heme-binding polypeptides with the axial ligands of bis-His and His/Met residues, respectively; DMSO, dimethyl sulfoxide; HPLC, high-performance liquid chromatography; MALDI-TOF, matrix-assisted laser desorption ionization time-of-flight; M_r, relative molecular mass; SHE, standard hydrogen electrode.

Covalent Attachment of Heme to Designed Apocytochromes. The *in vitro* reaction of protoheme with the polypeptide Cys residue was performed under mild reducing conditions according to the methods of Daltrop *et al*. (*21*, *22*). Concentrated apoproteins (1−1.5 mM) in 10 mM Tris-HCl (pH 8.0) were kept reduced by the addition of dithiothreitol (DTT) to a final concentration of 5 mM. Hemin (Sigma-Aldrich) solubilized in DMSO was diluted to 0.6 mM with 50 mM Tris-HCl (pH 8.0) and reduced with a small amount of sodium dithionite. Apo-designed cytochromes were added to the hemin solution in deaerated 50 mM Tris-HCl buffer (pH 8.0) at a final protein concentration of 0.2 mM. To fill the two heme binding sites of the designed cytochromes, hemin was added at approximately 2.5 equiv of protein. The reaction mixture was incubated in the dark under anaerobic conditions by a N_2 gas flow for 48−60 h. The reaction mixture was dialyzed against 0.05% TFA in the dark and was centrifuged to remove the insoluble materials. The supernatant was applied onto a C18 reverse-phase preparative HPLC column (COSMOSIL 5C18-AR300, Nacalai Tesque) and was eluted with a gradient of 30 to 50% (in cHH) and 37 to 52% (in cHM) acetonitrile in the presence of 0.05% TFA. The three-dimensional chromatograms were recorded in the wavelength range between 195 and 650 nm using a MD-1510 multiwavelength detector (JASCO). The peak fractions containing the designed cytochromes were collected, evaporated, and lyophilized. If necessary, reverse-phase chromatography was repeated to obtain a homogeneous protein fraction that was >95% pure. The samples were dissolved in water and dialyzed against an appropriate buffer solution. These procedures were carried out in the dark.

The covalent structures of synthesized polypeptides were identified by the visible absorption spectra of their pyridine hemochromes and also by MALDI-TOF mass spectrometry. Concentrations of heme *c*-binding designed cytochromes were determined by the absorption coefficient of pyridine hemochrome at the α peak (ϵ_{553}) estimated to be 30 mM^{-1} cm^{-1} (*24*).

Size-Exclusion Chromatography. Chromatography was performed on a Hitachi L-6200 HPLC system with a Hitachi L-4200 UV−visible detector or a JASCO MD-1510 multiwavelength detector using a Superdex75 gel filtration column (Pharmacia Biotech). It was operated with a mobile phase of 10 mM Tris-HCl (pH 8.0) and 200 mM NaCl at a flow rate of 1.0 mL/min. This column was standardized using commercially available globular proteins with a variety of masses and shapes (see Figure 2C).

Spectrometry. UV−visible absorption spectra of artificial cytochromes or these pyridine hemochromes were recorded with a Hitachi U-3000 spectrometer using quartz cuvettes with a path length of 1.0 cm. CD spectra were recorded at 20 °C with a JASCO J700 spectropolarimeter using quartz cuvettes with a path length of 0.2 cm. MALDI-TOF mass analyses were conducted with a Reflex mass spectrometer (Bruker Daltonics) using sinapinic acid as the matrix in the linear positive mode or an Ultraflex (Bruker Daltonics) in the positive MS/MS mode (*25*).

Redox Titration. To estimate the redox midpoint potentials, potentiometric titration was performed under anaerobic conditions with a continuous flow of gaseous nitrogen in TN buffer containing 10 mM Tris-HCl (pH 8.0) and 200 mM NaCl at 20 °C (*26*). The ambient redox potential was adjusted by the addition of sodium dithionite and potassium ferricyanide in the reductive and oxidative directions, respectively. The redox potential was measured with a combination MI-800-410 redox electrode (Microelectrodes, Inc.), and the optical absorption spectra were recorded throughout the titration on a Hitachi U-3000 spectrometer. The potentials measured against the Ag/AgCl reference electrode are reported against the standard hydrogen electrode (SHE) in the text. Equilibration between the electrode and the reaction mixture was facilitated with the following redox

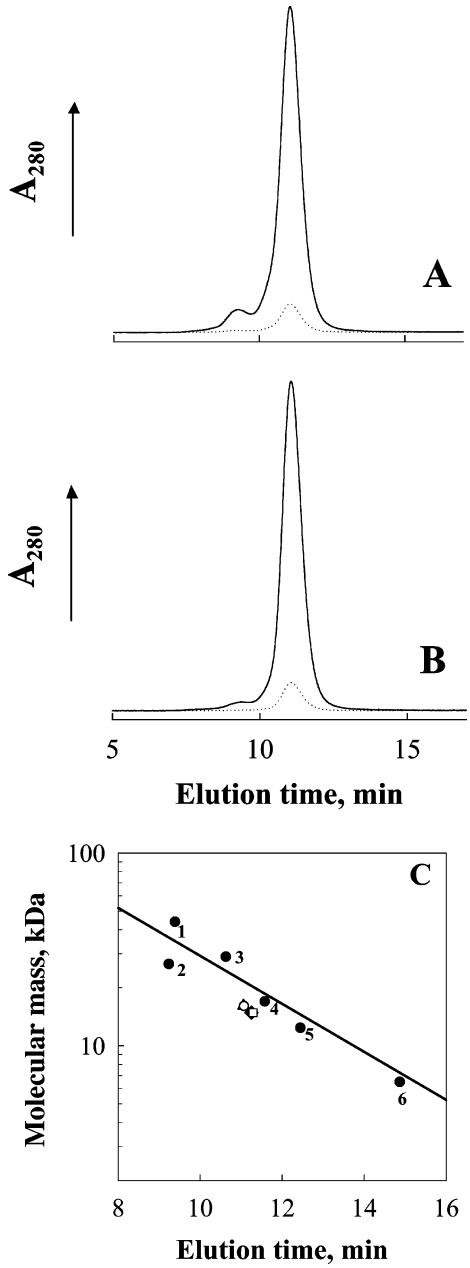

FIGURE 2: Size-exclusion chromatography of designed cytochromes *c*. The chromatograms of heme *c*-binding cHH (A) and heme *c*-binding cHM (B) were monitored via absorbance at 280 nm. A 50 μL aliquot of 10 μM (···) or 100 μM (—) proteins was loaded onto the column. Panel C gives the correlation between the molecular mass and elution time of $[apo\text{-}cHH]_2$ (◆), $[heme\ c\text{-}cHH]_2$ (▲), $[apo\text{-}cHM]_2$ (□), and $[heme\ c\text{-}cHM]_2$ (○), with that of natural globular proteins (●) with various M_r values and shapes: chicken ovalbumin (1), rabbit triosephosphate isomerase (2), bovine carbonic anhydrase (3), horse myoglobin (4), horse cytochrome *c* (5), and bovine aprotinin (6).

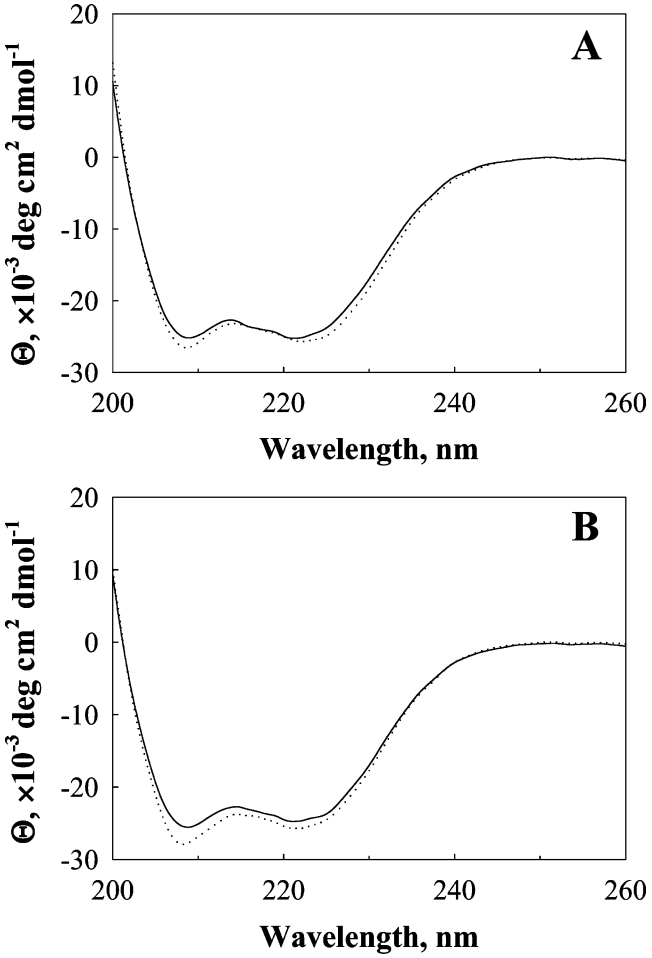

FIGURE 3: CD spectra of designed cytochromes *c*. The spectra of cHH and cHM are shown in panels A and B, respectively, in which the solid and dotted lines are for the apo and heme *c*-binding cytochromes, respectively. The spectra were recorded in 10 mM sodium phosphate (pH 8.0) and 200 mM NaCl at 20 °C. The protein concentrations were 10 μM as determined spectrophotometrically.

mediators at 10−30 μM: 2,3,5,6-tetramethyl-*p*-phenylenediamine, 1,4-naphthoquinone, 1,2-naphthoquinone, phenazine ethosulfate, phenazine methosulfate, duroquinone, and 2-hydroxy-1,4-naphthoquinone. Reduction of the heme was monitored by the increase in the α absorption bands. The titration data were analyzed by fitting the Nernst equation.

RESULTS

Synthesizing Artificial Cytochrome c. The amino acid sequences of artificial cytochrome *c* were constructed by modification of a designed helix−loop−helix polypeptide, which was originally designed to form the *b*-type heme-binding four-helix bundles in the dimer (*6*, *8*) as shown in Figure 1. These polypeptides, cHH and cHM, were efficiently expressed in their apo forms in the soluble fractions of recombinant *E. coli* cells. By mixing with protoheme in a buffer solution, the purified polypeptides bound the heme and exhibited UV−visible absorption spectra characteristic of *b*-type cytochromes (see Figure 4). The *b*-type heme-binding polypeptides were incubated for 2−3 days under mild reducing conditions, and the fractions with covalently attached heme were collected by reversed-phase HPLC under denaturing acidic conditions (see Materials and Methods). To verify the formation of the covalent bond between the heme and polypeptides, pyridine hemochrome and MALDI-TOF mass spectra were measured. The pyridine hemochrome spectra of the heme-attached polypeptides showed the α bands at 553 nm, indicating *c*-type heme with a single thioether bond, as in the case of *Euglena gracilis* and *Crithidia oncopelti* cytochromes *c* (*24*), whereas these spectra of the heme *b*-binding intermediates showed the α bands of 556 nm characteristic of *b*-type hemoproteins. The mass analyses revealed that the attachment of heme to cHH and cHM increased the mass values by 617 and 618 Da, respectively, both of which are identical to the mass of iron protoporphyrin IX ($C_{34}H_{32}O_4N_4Fe$, 616.5 Da) within the instrumental error, and that the heme-attached cHH and cHM proteins have masses of 8049 and 8043 Da, respectively, which correspond to the calculated values of the heme-attached cHH (8048.5 Da) and cHM (8042.6 Da) (Table 1). Furthermore, digestion of these holocytochromes by *Achromobacter* protease I (*27*) produced heme-attached peptide fragments with a mass of 1511.6 Da which is identical to the calculated mass (1511.7 Da) of the heme-attached KFEECLK. Thus, these polypeptides have a covalent linkage to the heme via a single cysteine residue as designed. On the other hand, any covalent attachment of heme to bHH, which has no Cys residue in the sequence, did not occur by incubation of the polypeptide with heme under the same reducing conditions.

The purified, heme-attached polypeptides recovered in the reversed-phase HPLC were refolded in a buffer solution at a neutral pH and were used for the following analyses.

Four-Helix Bundle Formation. Self-association of the designed cytochromes *c* was analyzed by size-exclusion chromatography, in which the elution volume of a protein depends on both the size and molecular shape (Figure 2). In the chromatography of the heme *c*-binding proteins, the main peaks were eluted in the M_r range of the dimer over the loading protein concentrations of 10 and 100 μM, whereas the larger aggregate appeared as the minor peak at a higher loading protein concentration (Figure 2A, B). The major peak was identified as a dimer, based on a standard curve derived from the data of globular proteins as shown in Figure 2C. The main fractions of the apoproteins were also eluted as the dimer (Figure 2C), and thus, the attached heme has little effect on the association states.

Secondary structures of the apo forms of the designed cytochromes were probed by far-UV circular dichroism (CD) measurements (Figure 3). The CD spectra of these proteins indicate the highly α-helical features of their structures and that the sequence modification in cHH and cHM results in only minor changes in the helical content in comparison with the original protein [α-*l*-α]$_2$ (*8*). Both the mean residue ellipticities of apo-cHH and apo-cHM were determined to be (−2.5 ± 0.1) × 10^4 deg cm^2 dmol^{-1} at 222 nm. On the other hand, those of the heme *c*-binding cHH and cHM were determined to be (−2.6 ± 0.1) × 10^4 deg cm^2 dmol^{-1} at 222 nm. From these values, all the helical contents of the apo- and holocytochromes were identical within experimental error and were estimated at approximately 80% based on the ellipticity of −32000 deg cm^2 dmol^{-1} for 100% helicity (*28*), as summarized in Table 1. Thus, the covalent attachment of heme produced almost no effects on the helical contents of cHH and cHM. Also, the ratio of signal intensity at 222 and 208 nm showed no significant changes in these

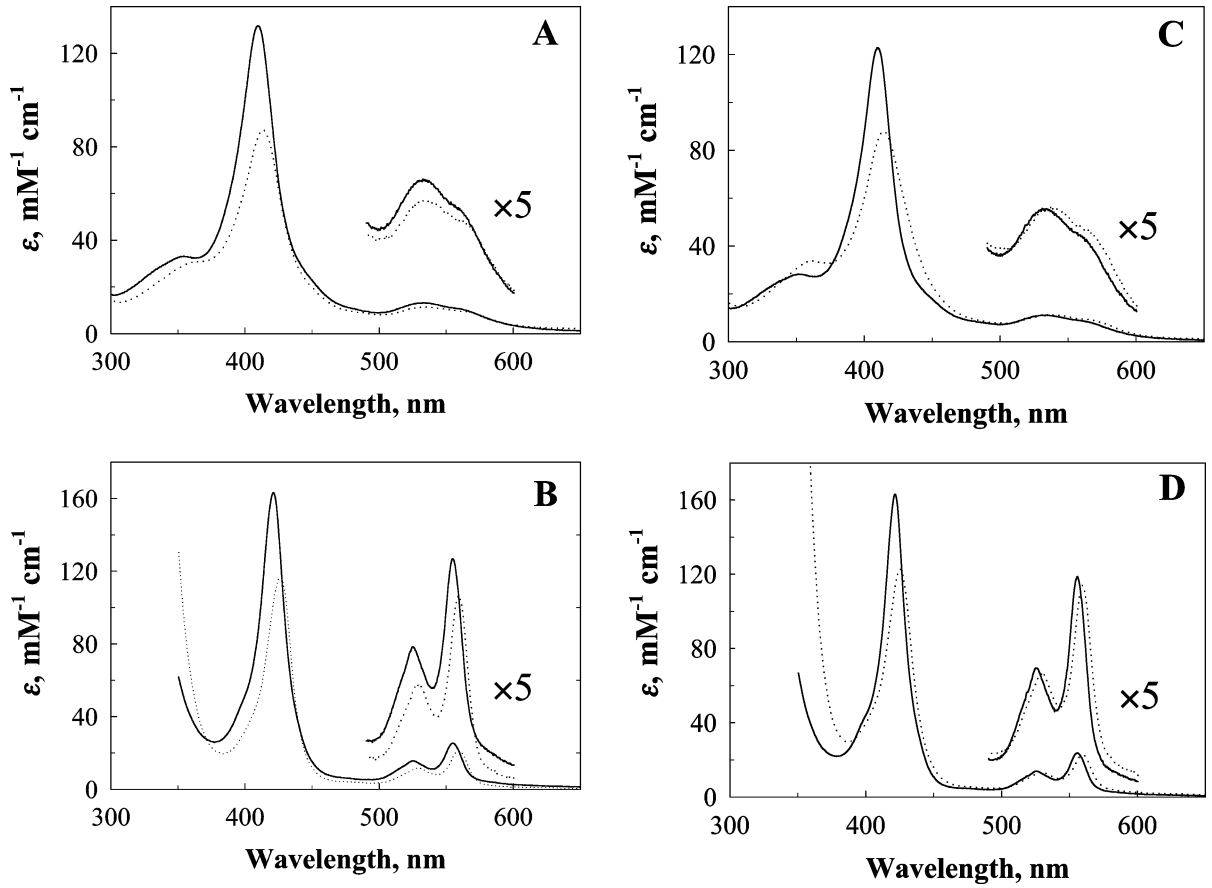

FIGURE 4: UV−visible absorption spectra of artificial holocytochromes. Panels A and B show the spectra of holo-cHH in the ferric and ferrous forms, respectively. Panels C and D show the spectra of holo-cHM in the ferric and ferrous forms, respectively. The absorption bands of the heme *c*-binding cytochromes (—) shifted to a shorter wavelength compared to those of their heme *b*-binding intermediates (···). The absorbance increases of the ferrous forms around 350 nm in panels B and D were due to sodium dithionite added for the reduction of heme. These spectra were recorded in 10 mM Tris-HCl (pH 8.0) and 200 mM NaCl at protein concentrations of 5 μM at 20 °C.

Table 1: Mass and CD Analyses of Apo and Heme *c*-Binding Forms of Synthesized Artificial Cytochromes

	molecular mass (Da)		mean residue ellipticity (deg cm^{-2} dmol^{-1})[b]			
protein	calcd	measured[a]	θ_{222}	θ_{208}	$\theta_{222}/\theta_{208}$	% α helix
apo-cHH	7432.0	7432	−25226	−24760	0.97	78.2
heme *c*-cHH	8048.5	8049	−25685	−26411	0.97	80.8
apo-cHM	7426.1	7425	−25035	−25385	0.99	78.2
heme *c*-cHM	8042.6	8043	−25859	−28043	0.92	80.8

[a] The instrumental errors are ±0.1% of the measured values. [b] The data represent mean values of three separate measurements with a standard deviation of ±3%.

Table 2: Spectral and Electrochemical Properties of Artificial Cytochromes

protein	oxidized Soret, β, α bands (nm)	reduced Soret, β, α bands (nm)	E_m (mV vs SHE)
cHH			
heme *c*	409.5, 532.5	421.0, 525.0, 554.5	−105, −220
heme *b*	414.0, 535.5	426.0, 529.5, 559.5	ND[a]
cHM			
heme *c*	409.5, 534.0	421.5, 525.5, 556.0	−90, −187
heme *b*	414.5, 537.5	425.5, 529.0, 559.5	−105, −214

[a] Not determined.

proteins (Table 1), suggesting that the coiled-coil supersecondary structures are not affected by the heme *c* binding.

Heme Spectroscopy. Absorption spectra of the holo forms of cHH and cHM (Figure 4) indicate that both the polypeptides bind hemes in a low-spin six-coordinated state. In the oxidized forms, both the heme *c*-binding cHH and cHM proteins exhibited a Soret peak at 409.5 nm. These peaks are at wavelengths shorter than those of the heme *b*-binding intermediates of cHH and cHM by approximately 5 nm (Table 2). On the other hand, the reduced forms of the heme *c*-binding cHH and cHM exhibited the α, β, and Soret peaks at 554.5, 525.0, and 421.0 nm and at 556.0, 525.5, and 421.5 nm, respectively. These values are at wavelengths shorter than those of the heme *b*-binding intermediates of cHH and cHM by approximately 5 and 4 nm, respectively (Table 2). These blue shifts of the absorption bands by the covalent attachment of heme to the polypeptides agree with the differences in the spectral features between natural *b*- and *c*-type cytochromes and also with the mutational conversion of cytochromes *b* to *c* (*19*, *20*) and *vice versa* (*22*, *29*, *30*) (Table 3). Furthermore, the introduction of a thioether bond between heme and the polypeptide increased the absorption coefficients and sharpened the band shapes, suggesting the restriction of the conformational geometry of the heme inside the protein molecule.

Redox Titration. Redox properties of the designed cytochromes were studied in equilibrium redox titration. Figure 5 shows changes in the fraction of the reduced heme assayed by optical spectroscopy as a function of the solution redox potentials for each of the proteins. The titration curves are biphasic due to the fact that the two hemes are associated

Table 3: Spectral and Electrochemical Properties of Natural Cytochrome Variants Converted from the *b* to *c* Type and *Vice Versa*

protein	axial ligands	heme *c*-binding motif	thioether bond	reduced absorption maximum Soret, β, α bands (nm)	reduction potentials (mV vs SHE)	refs
bovine liver cytochrome b_5	bis-His (wild type)	−	−	423, 527, 555	+4[c]	*19*, *31*
	His/Met[a]	−	−	ND[e]	ND[e]	
	bis-His	−	single[b]	420, 527, 555.5	−19[c]	
E. coli cytochrome b_{562}	His/Met (wild type)	RNAYH	−	426.5, 531.0, 561.5	+165[c]	*20*, *32*, *33*
	bis-Met	RNAYM	−	430, 530, 561.5	+240[c]	
	bis-Met	CNAYM	single	426, 528, 557	+350[c]	
	His/Met	CNAYH	single	421.5, 527.5, 556	ND[e]	
	His/Met	RNACH	single	424.5, 529.5, 560.5	ND[e]	
	His/Met	CNACH	double	421, 526, 556	ND[e]	
	His/Met	CNACH	single	424, 529, 559.5	ND[e]	
H. thermophilus cytochrome c_{552}	His/Met (wild type)	CMACH	double	417, 521, 552	+245[d]	*21*, *29*, *30*, *34*
	His/Met	CMAAH	single	420, 525, 556	+250[d]	
	His/Met	CMAAH	−	424, 528, 559	ND[e]	
	His/Met	AMACH	single	418, 526, 558	+225[d]	
	His/Met	AMACH	−	425.5, 528.5, 559.5	ND[e]	
	His/Met	AMAAH	−	425, 529, 560	+170[d]	
	His/Met	CMACH	−	425, 530, 560	ND[e]	*35*, *36*
T. thermophilus cytochrome c_{552}	His/Met (wild type)	CAGCH	double	417, 525, 552	ND[e]	
	His/Met	CAGCH	single	423, 526, 557	ND[e]	
P. denitrificans cytochrome c_{550}	His/Met (wild type)	CKACH	double	415, 521.5, 550	ND[e]	*22*
	His/Met	CKACH	−	423, 528.5, 558.5	ND[e]	
horse cytochrome *c*	His/Met (wild type)	CAQCH	double	415, 520, 550	+262[d]	*22*, *37*
	His/Met	CAQCH	−	424, 528, 559	ND[e]	
	bis-His	CAQCH	double	415, 520, 550	+41[d]	
yeast iso-1-cytochrome *c*	His/Met (wild type)	CLQCH	double	415, 518.5, 549	+282[c]	*38*, *39*
	His/Met	SLQCH	single	418, 522, 553	ND[e]	

[a] Methionine sulfur is not bonded to the heme iron, and the bound heme is five-coordinated. [b] The heme is not attached at the heme *c*-binding motif but at the Cys replacing Asn-57 of the wild type, which is close to a heme vinyl group in the tertiary structure. [c] Determined by cyclic voltammography. [d] Determined by equilibrium redox titration. [e] Not determined or not reported.

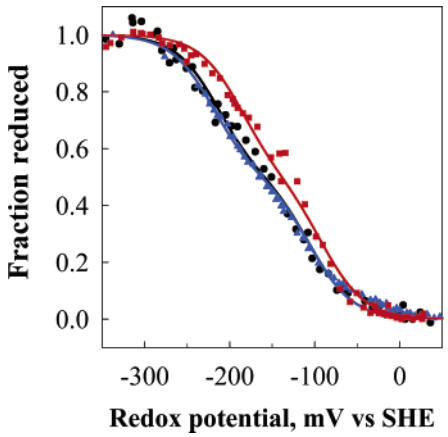

FIGURE 5: Redox titration of artificial cytochromes. The fractions of the reduced forms of heme *b*-binding cHM (black circles), heme *c*-binding cHH (blue triangles), and heme *c*-binding cHM (red squares) were plotted against the solution redox potentials under equilibrium conditions. The data were obtained from the spectral changes of the cytochromes in the α- and β-band region with the potential monitored by a combination redox electrode at 20 °C. The theoretical curves were drawn by fitting the data using two independent Nernst equations ($n = 1$).

with the four-helix bundle dimer (*6*, *8*). Thus, the data were fitted using the two independent Nernst equations, each with one electron transition ($n = 1$), to estimate the midpoint redox potentials (E_m). The E_m values of the heme *b*-binding intermediate of cHM were determined to be -105 ± 10 and -214 ± 10 mV (Table 2). These values were identical to the values of −100 and −215 mV of the original designed four-helix bundle (IIb_2 or $[H10A24]_2$) with protoheme bound by bis-His ligation (*6*) within experimental error. This is a reasonable coincidence because protoheme is not associated with cHM at the heme *c*-binding site by the His/Met ligation but associated at the heme *b*-binding site by the bis-His ligation near the loop (see Figure 1 and the Discussion). The E_m values of heme *c*-binding cHH and cHM were determined to be -105 ± 10 and -220 ± 10 mV, and -90 ± 10 and -187 ± 10 mV, respectively (Table 2). Thus, the covalent attachment of heme to the polypeptide with the bis-His axial ligation did not affect the redox potential, but the combination of the covalent attachment with the replacement of the bis-His ligation with the His/Met ligation gives redox potentials higher by 15−30 mV in these artificial systems. These results for redox properties contrast with those of the conversion of natural cytochromes *b* to the *c*-type variants (*19*, *20*) and of natural cytochromes *c* to the *b*-type variants (*22*, *29*, *30*) (see Table 3 and the Discussion).

DISCUSSION

The research goal of protein design is the construction of novel amino acid sequences capable of folding into a functional tertiary structure. In the design of cytochromes, the ability to control the midpoint redox potentials is an important measure for assessment of the function. The previously designed heme-binding proteins exhibited potentials lower than those of native cytochromes; e.g., the *a*-type heme binding maquette protein has the most positive potential [but only 40 mV versus SHE (*40*)], whereas native cytochromes have a variety of potential values of up to 400 mV. We consider that the difficulty in making heme proteins with higher potentials is partly due to the creation of a hydrophobic environment around the bound heme, which requires unique side chain packing inside the protein core containing heme. This is closely related to the general and difficult subject of protein design, i.e., achievement of a

native-like unique structure. Many artificial proteins with the secondary structures and the overall topology successfully designed exhibited mixed conformational states or a "gemisch" state (*41*), which is similar to molten globules of native protein folding intermediates, but never achieved any single structures under any conditions. In such a multiple-conformation state of a heme protein, water molecules easily enter into the protein core, and the hydrophobic environment cannot be attained as in native protein cores. The favorable interaction between water and ferric heme with net charge of +1 stabilizes the oxidized form to shift the redox equilibrium in the oxidized direction. Thus, the redox potential of an artificial heme protein is an essential probe for the native-like structure coupling with the function. The artificial cytochromes *c* also provide a useful system for controlling the redox potential via the stability modulation because the covalent linkage to the heme prevents its release when the oxidized form is destabilized and makes effects of the lower heme affinity negligible.

The artificial cytochromes *c*, cHH and cHM, follow the amino acid sequence designed to form multi-heme-binding proteins (*6*, *8*) and preserve the heme *b*-binding site formed by His-23 and His-42, which are assumed to face each other in the helix bundle, in addition to the heme *c*-binding site formed by His-9 (Met-9) and His-56 (see Figure 1). Thus, they have the two heme *c*-binding sites and also have the two extra heme *b*-binding sites in the four-helix bundle dimer. The heme *c* sites correspond to the 24, 24′ position in the original H10H24 or α-SS-α polypeptide (*6*, *8*) and should have the binding affinity for protoheme, which is lower than that of the heme *b* sites corresponding to the 10, 10′ position near the loop region. After the formation of the thioether bond between the heme and the Cys residue in the heme *c* site with excess heme, the heme without the covalent bond was removed from the polypeptides during the purification procedures. Thus, the resulting proteins preserved the two vacant heme *b*-binding sites in the four-helix bundle. We have tried to prepare proteins binding both hemes *b* and *c* in a single molecule by adding protoheme to the heme *c*-attached cHM. In the binding titration experiments with the heme *c*-attached polypeptide, however, almost no heme *b* binding was observed under low concentrations of added heme and the dissociation constant of the holocytochrome *c* for protoheme was more than several micromolar. Interestingly, at higher concentrations of heme, the axial ligation of heme *c* was gradually lost whereas small amounts of heme *b* were bound (not shown). This may be due to the direct steric interference between the hemes as previously suggested in the original four-helix bundle with heme *a* (*40*), and/or due to indirect negative cooperation between binding of heme *b* and that of heme *c*; i.e., the binding of heme *b* induces unfavorable conformational changes for heme *c* binding, and *vice versa* (also see below).

In the apo and heme *b*-binding forms, there are at least seven possible topologies of our four-helix bundles, as shown in Figure 6. These topologies can be classified by the three arrangements of the loops (syn, anti, and bisecting) (*42*) and also by the four arrangements of the helix dipoles (I−IV). The syn, anti, and bisecting topologies can have three, two, and two helix−dipole arrangements, respectively (Figure 6). In the syn-II and anti-II topologies, the monomers with the same sequences have conformations different from each other, and these topologies should be rare. On the other hand, the bound heme *c* restricts the topologies to three species (syn-I, anti-I, and bisecting-II) by fixing the helix disposition in an interface between the helices. The bisecting topologies are impossible in the four-helix bundles without the heme *b* binding sites near the loop, such as the polypeptides with Ala residues for His-23 and His-42.

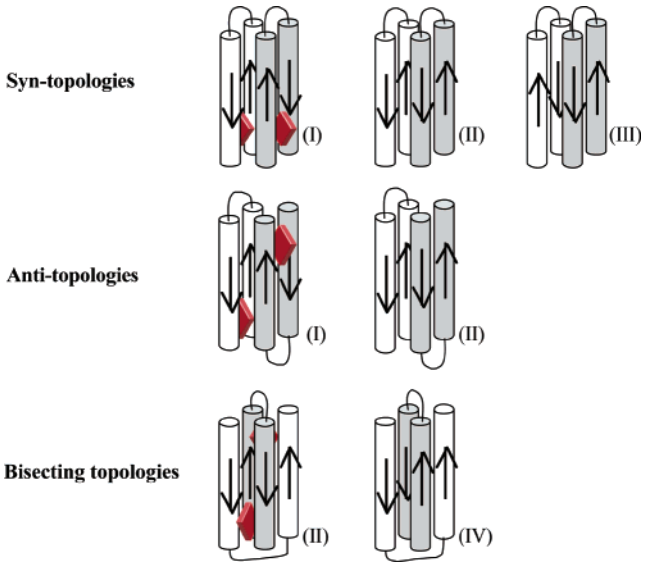

FIGURE 6: Possible topologies of the dimer four-helix bundles. The topologies are classified by the arrangements of the loops with the same (syn) and opposite (anti) sides of the bundle and of the loops bisecting at the opposite sides of the bundle, and also by the arrangements of the helix dipoles (I−IV) indicated by the arrows from the amino- to carboxyl-terminal ends of the helices. The bisecting syn topologies should be rare for steric hindrance between the loops and are excluded from this set of topologies. In the heme *c*-binding forms with the bis-His or His/Met ligation, only helix−dipole arrangements I, I, and II are possible for the syn, anti, and bisecting topologies, respectively, as shown in the figure. Red square plates represent the bound heme *c*.

The splits of the midpoint potentials observed in the redox titration of the heme *c*-binding cHH and cHM were approximately 100 mV (Figure 5 and Table 2), suggesting the electrostatic interactions between the two bound hemes within the four-helix bundle (*6*, *8*, *40*, *43*, *45*). The entropic effect on the difference in redox potentials between two noninteracting redox centers bound to a protein molecule can be estimated via $(2RT/F) \ln 2 = 35.6$ mV at 25 °C, arising from the fact that donation of the first electron to a molecule with two oxidized redox centers occurs more easily (at a higher potential) than that of the second electron to the molecule with only one oxidized center (at a lower potential) (*46*, *47*). Thus, the residual potential difference, 60−80 mV, can be attributed to the electrostatic repulsion between the ferric hemes in the holocytochromes *c*. As mentioned above, we have constructed several three-dimensional models of the artificial cytochromes *c* with different topologies and favor the anti-I topology rather than the others, because this topology is most symmetrical and produces less steric hindrance between the bound hemes (see Figure 6). The distance between the bound heme *c* centers in the anti-I topology is estimated to be 17−20 Å based on the X-ray structure of a designed four-helix bundle variant in another anti topology (*48*). This distance is equivalent to a potential difference in a range of only 10 mV in the hydrophobic interior of a natural globular protein (*49*) but may correspond

to larger values in the less hydrophobic (higher dielectric) interior of the artificial proteins.

The two distinct components observed in the redox titration have been assumed to arise from the electrostatic interactions between the bound hemes that are close to each other in the syn topology of the four-helix bundles. However, there is only a small energetic difference between the syn and anti topologies (*45*, *50*), and the recently revealed X-ray structure of a four-helix bundle maquette in the apo form has the anti topology (*48*). Furthermore, introduction of protohemes into the syn topology induces unfavorable effects for this orientation and shifts the topological balance to the anti orientation by 25−50-fold (*45*). This shift was more significant in binding of heme *a* with the longer side chain due to the steric effect (*40*), which may be similar in the case of conformationally more restricted heme *c*.

E. coli cytochrome b_{562}, which is a four-helix bundle hemoprotein containing a six-coordinated heme iron ligated by His and Met residues, was converted to the *c*-type cytochromes by replacing R98 and/or Y101 at the positions close to His102, one of the axial ligands of heme iron, with Cys to generate the Cys-X-X-Cys-His, Arg-X-X-Cys-His, and Cys-X-X-Tyr-His motifs in the *b*-type cytochrome and by *in vivo* synthesis (*20*, *32*, *33*) (Table 3). These cytochrome b_{562} variants with the His/Met ligation have the covalently attached *c*-type heme with the single or double thioether bonds and exhibit blue shifts of the absorption bands, e.g., from the α band of the wild-type reduced form at 561.5 nm to that of the Cys-X-X-Cys-His variant with the double thioether bonds at 555.5 nm (*20*). Bovine liver cytochrome b_5 was also converted to the *c*-type cytochrome without a change in the bis-His axial ligands (*19*), which showed spectral changes similar to those of cytochrome b_{562} (*20*). Furthermore, the inverse spectral shifts to lower energy were observed in the conversion of the natural cytochromes *c* to *b*-type cytochrome variants (Table 3). These results agree with the spectral differences between the heme *b*- and heme *c*-binding forms of our designed cytochromes (Figure 4 and Table 2) and confirm the formation of the covalent bond between heme and the polypeptides, which had been evidenced by the mass spectrometric analyses and their pyridine hemochrome spectra (see the Results).

The increases in absorption band intensity caused by formation of the covalent bond (Figure 4) suggest that the thioether bond imposes conformational restriction on the bound heme and increases a single state of the bound heme. These absorption spectra of the holocytochromes *c* clearly indicated that these proteins have six-coordinated low-spin hemes as designed. In contrast to natural monoheme binding cytochromes, our artificial cytochromes have two heme-binding sites in the helix−loop−helix monomer; i.e., in the four-helix bundle, cHH has four bis-His sites and cHM has both two bis-His sites and two His/Met sites. As mentioned above, the bis-His heme *b*-binding sites close to the loop region have higher affinity for protoheme than the other bis-His and His/Met heme *c* binding sites in cHH and cHM, respectively. Thus, it should be noted that these artificial cytochromes bind protoheme at the heme *b* sites rather than the heme *c* sites in the intermediates, and the spectral and redox data for the heme *b*-binding intermediates concern the binding sites different from those of the heme *c*-binding cytochromes.

The heme *c* with bis-His ligation in cHH has redox potentials of −105 and −220 mV at pH 8.0 (Table 2). These values are very similar to those of bis-His-ligated heme *b* at the high-affinity 10, 10′ sites of the prototype four-helix bundle (IIb_2 or $[H10A24]_2$), i.e., −100 and −215 mV at pH 8.0 (*6*, *8*) and −144 and −216 mV at pH 8.5 (*43*). The cHM-bound heme *c* with His/Met ligation exhibited a potential 10−30 mV higher than that of the cHH-bound heme *c* (Table 2). Moreover, the heme *b*-binding intermediate of cHM, which contained approximately 1.0 equiv of protoheme per monomer and was expected to bind the heme with bis-His ligation at the heme *b* site near the loop, exhibited redox potentials of −105 and −214 mV, similar to those of the cHH-bound heme *c*. Thus, we conclude that the thioether bond between the heme and polypeptide does not affect the redox potential in the designed cytochromes and that the replacement of the bis-His ligation with the His/Met ligation increases the potential. However, the potential increase by axial ligand replacement is small, and the redox potentials of heme *c* with His/Met ligation in cHM (−90 and −187 mV) are still much lower than those of natural cytochromes *c* and their variants with either single or double thioether bonds (170−350 mV) (Table 3). Therefore, the higher redox potentials of natural cytochromes *c* can be attributed not only to the covalent structures around the heme, including both the His/Met ligation and the thioether bonds, but also to the noncovalent and hydrophobic environments formed by their amino acid sequences; i.e., the heme coordination structure as well as the covalent attachment to polypeptide should be essential but not enough for realization of the higher redox potentials characteristic of natural cytochromes *c*.

Hydrogenobacter thermophilus cytochrome c_{552} has a normal heme *c*-binding motif (CXXCH) with the double thioether bonds and the His/Met ligation. Tomlinson and Ferguson (*29*, *30*) reported that the AXXCH and CXXAH variants of this cytochrome with the single thioether bond preserved thermal stability and redox potentials that were almost the same as those of the wild type, whereas the AXXAH variant without any thioether bond is less stable than the wild type and the redox potential reduced by 75 mV (Table 3). From these results, the authors inferred that the potential drop was caused by the change in the heme environment along with the loss of stability rather than the change in the covalent structure of heme and that either of the thioether bonds contributes to the stability but contributes little to the redox potential. This conclusion is consistent with our results using the artificial system. On the other hand, Barker *et al.* (*32*) reported that a bis-Met variant of *E. coli* cytochrome b_{562} with a single thioether bond had a substantially higher redox potential than another bis-Met variant of this cytochrome with no thioether bond, as shown in Table 3. Thus, in this case, the thioether bond contributes to the increase in the potential. Mechanisms underlying this effect of the covalent bond are not clear (*32*) but may correlate with the combination of the thioether bond with the axial ligand arrangement as well as the other environments surrounding heme.

The potentials of redox proteins are determined by the differences in thermal stability between the oxidized and reduced forms, and the oxidized form of a higher-potential protein is less stable than the reduced form. For example, the reduced form of cytochrome c_{556} from *Rhodopseudo-*

monas palustris is more stable toward unfolding than the oxidized form ($\Delta\Delta G_f^\circ = \sim 22$ kJ/mol), and the redox potential is 220 mV (*51*). On the contrary, a single heme *c* bound to cHM in the folded state is assumed to have a redox potential near −190 mV (see Figure 5 and Table 2), which is equivalent to 18.7 kJ/mol. Thus, the oxidized form is more stable than the reduced form by the same energy (18.7 kJ/mol) for the folding−unfolding transition, assuming that the redox potential in the unfolded state is 0 mV. The higher stability of the oxidized form can be attributed to the preferable interaction between the ferric heme (Fe^{3+}) with the center net charge of +1 and water molecules that invaded the protein interior. Thus, the redox potentials of the artificial cytochromes can be increased by making the heme environment more hydrophobic. In natural *c*-type cytochromes with higher redox potentials, the covalent attachment to the polypeptide prevents loss of the heme despite the considerably low stability in the ferric states and indirectly contributes to the higher redox potentials by maintaining the holo forms. Therefore, our artificial cytochromes *c* can be redesigned to increase the redox potential by decreasing the thermal stability without the loss of heme and provide a good system for investigating the functional control of heme proteins.

At the beginning of this study, we synthesized a polypeptide with a normal heme *c*-binding motif with two Cys residues (Cys-Leu-Lys-Cys-His) in place of the motif with one Cys residue (Cys-Leu-Lys-Leu-His) in cHH, and applied them to the reaction with heme. However, we have failed to obtain a homogeneous preparation of the CXXCH holocytochrome *c* with the double thioether bonds. The purified fraction of the CXXCH cytochrome as a single peak of the reversed-phase HPLC exhibited an α absorption peak at 554.5 nm in the reduced form, which was identical to that of the cHH polypeptide (see Table 2). Furthermore, the pyridine hemochrome spectrum of the CXXCH cytochrome showed an α peak at 551.6 nm, which is slightly smaller than that of the cHH cytochrome at 553 nm but larger than 550 nm which is the value expected for the double thioether bonds. Thus, the CXXCH cytochrome preparation seemed to contain a mixture of polypeptides with single and double thioether bond(s). In the CXXCH cytochrome with a single thioether bond, there might be the heterogeneous species with all the combinations of a bond between one of the two Cys residues and one of the two vinyl groups of heme. Furthermore, formation of intermolecular disulfide bonds between polypeptides easily occurred since nonreacted free Cys residues remain in the polypeptides after the reaction with heme. Thus, the molecules obtained from the CXXCH polypeptide were highly heterogeneous and cannot be separated by our purification procedures. A polypeptide with another single Cys sequence, Leu-Leu-Lys-Cys-His, was also synthesized and reacted with heme. In this reaction, the yield of heme attachment was very low and substantial amounts of the molecule were not obtained for characterization. The low yield of bond formation agrees with reports on a *H. thermophilus* cytochrome c_{552} variant with a Ala-Met-Ala-Cys-His sequence (*30*) and a mitochondrial cytochrome *c* variant with a Ser-Leu-Gln-Cys-His sequence (*38*). The low yield of the heme attachment of our XXXCH polypeptide as well as the natural cytochrome variants may be due to the fact that the more distorted or energetically unfavorable configuration of side chains and/or backbone of the heme *c* binding motifs is forced by the linkage of heme to the Cys residue next to the His residue in comparison with that to the other Cys residue apart from the His residue. Thus, we selected the Cys-Leu-Lys-Leu-His sequence for binding heme *c* and successfully synthesized *de novo* cytochromes *c* with the simple artificial amino acid sequences (see Figure 1). At present, we cannot identify which vinyl group at the second or fourth position of the heme was attached to the polypeptide and assume that the products were mixtures of heme *c* with a bond at either of both the positions because the polypeptides were not designed to select the heme geometry.

Also early in this study, we have attempted to attach heme to designed polypeptides with the Cys-X-X-Cys-His sequence at the carboxyl-terminal region and with the pelB signal sequences at the amino terminus, using an *in vivo* system with a cytochrome *c* maturation (*ccm*) gene cluster transformed into *E. coli* (*18*). In this biosynthetic system, formation of the thioether bonds in native recombinant cytochromes *c* efficiently occurs in the periplasmic space, into which the apoproteins were transported after expression in the cytoplasm. However, our designed polypeptides were not transferred to the periplasmic space across the plasma membrane even though several signal sequences were tried, and no heme *c*-bound proteins were synthesized. This failure seems to be due to their stable secondary structures in the apo forms (see refs *8*, *43*, and *44*). Consequently, we adopted the *in vitro* method of Daltrop *et al.* (*21*, *22*) for synthesizing the artificial cytochromes *c*.

There have been arguments about the chemical and biological mechanisms for the cytochrome *c* maturation or the correct attachment of heme to the proteins. McRee *et al*. (*36*) demonstrated that the proper maturation of recombinant cytochrome c_{552} from *Thermus thermophilus* in *E. coli* cells required the coexpression of the native signal peptide preceding the amino terminus of the cytochrome (also see Table 3). Allen *et al*. (*33*) showed that the correct maturation of an *E. coli* cytochrome b_{562} variant with a CXXCH motif occurred in the presence of the native *ccm* apparatus and that the *in vitro* spontaneous formation of the covalent bond in the absence of *ccm* produced an improperly matured cytochrome with an incorrect orientation of the heme (Table 3). These results suggest that the biological apparatus are required for the correct cytochrome *c* maturation and contrast with the *in vitro* maturation described by Daltrop *et al*. (*21*, *22*, *34*). These different results for the requirement of the biogenesis system for cytochrome *c* maturation may depend on the cytochrome species and the synthetic procedures. Our artificial cytochromes may provide an unbiased system for investigating the chemical and biological mechanisms for cytochrome *c* maturation. However, the designed cytochromes *c* presented here bind two hemes interacting with each other in the four-helix bundle and are not suitable for detailed analyses of the geometry of the bound heme. For this purpose, we are now synthesizing new cytochromes binding a single heme per four-helix bundle.

ACKNOWLEDGMENT

We thank Ms. Yasue Ichikawa and Ms. Rie Nakazawa for DNA sequencing (Bioarchitect Research Group, RIKEN), Ms. Tomoe Nishimura for mass spectrometry measure-

ments (Biomolecular Characterization Team, RIKEN), Dr. Takeharu Masaki (Ibaraki University) for his kind gift of *Achromobacter* protease I, and Drs. Tadashi Satoh and Shin-ichi Adachi (Institute of Materials Structure Science, KEK) for helpful discussion.

REFERENCES

1. DeGrado, W. F., Summa, C. M., Pavone, V., Nastri, F., and Lombardi, A. (1999) De novo design and structural characterization of proteins and metalloproteins, *Annu. Rev. Biochem. 68*, 779−819.
2. Kennedy, M. L., and Gibney, B. R. (2001) Metalloprotein and redox protein design, *Curr. Opin. Struct. Biol. 11*, 485−490.
3. Desjarlais, J. R., and Handel, T. M. (1995) New strategies in protein design, *Curr. Opin. Biotechnol. 6*, 460−466.
4. Bryson, J. W., Betz, S. F., Lu, H. S., Suich, D. J., Zhou, H. X., O'Neil, K. T., and DeGrado, W. F. (1995) Protein design: a hierarchic approach, *Science 270*, 935−941.
5. Cordes, M. H. J., Davidson, A. R., and Sauer, R. T. (1996) Sequence space, folding and protein design, *Curr. Opin. Struct. Biol. 6*, 3−10.
6. Robertson, D. E., Farid, R. S., Moser, C. C., Urbauer, J. L., Mulholland, S. E., Pidikiti, R., Lear, J. D., Wand, A. J., DeGrado, W. F., and Dutton, P. L. (1994) Design and synthesis of multihaem proteins, *Nature 368*, 425−432.
7. Choma, C. T., Lear, J. D., Nelson, M. J., Dutton, P. L., Robertson, D. E., and DeGrado, W. F. (1994) Design of a heme-binding four-helix bundle, *J. Am. Chem. Soc. 116*, 856−865.
8. Gibney, B. R., Rabanal, F., Reddy, K. S., and Dutton, P. L. (1998) Effect of four helix bundle topology on heme binding and redox properties, *Biochemistry 37*, 4635−4643.
9. Rabanal, F., DeGrado, W. F., and Dutton, P. L. (1996) Toward the synthesis of a photosynthetic reaction center maquette: A cofacial porphyrin pair assembled between two subunits of a synthetic four-helix bundle multiheme protein, *J. Am. Chem. Soc. 118*, 473−474.
10. Isogai, Y., Ota, M., Fujisawa, T., Izuno, H., Mukai, M., Nakamura, H., Iizuka, T., and Nishikawa, K. (1999) Design and synthesis of a globin fold, *Biochemistry 38*, 7431−7443.
11. Isogai, Y., Ishii, A., Fujisawa, T., Ota, M., and Nishikawa, K. (2000) Redesign of artificial globins: effects of residue replacements at hydrophobic sites on the structural properties, *Biochemistry 39*, 5683−5690.
12. Moore, G. R., and Pettigrew, G. W. (1990) in *Cytochromes c: Evolutionary, Structural and Physicochemical Aspects* (Rich, A., Ed.) Springer-Verlag, Berlin.
13. Barker, P. D., and Ferguson, S. J. (1999) Still a puzzle: why is haem covalently attached in *c*-type cytochromes? *Struct. Folding Des. 7*, R281−R290.
14. Boehning, D., Patterson, R. L., Sedaghat, L., Glebova, N. O., Kurosaki, T., and Snyder, S. H. (2003) Cytochrome *c* binds to inositol (1,4,5) trisphosphate receptors, amplifying calcium-dependent apoptosis, *Nat. Cell Biol. 5*, 1051−1061.
15. Sambongi, Y., Yang, J. H., Igarashi, Y., and Kodama, T. (1991) Cloning, nucleotide-sequence and expression of the cytochrome c_{552} gene from *Hydrogenobacter thermophilus*, *Eur. J. Biochem. 198*, 7−12.
16. Thöny-Meyer, L., Fischer, F., Kunzler, P., Ritz, D., and Hennecke, H. (1995) *Escherichia coli* genes required for cytochrome *c* maturation, *J. Bacteriol. 177*, 4321−4326.
17. Patel, C. N., Lind, M. C., and Pielak G. J. (2001) Characterization of horse cytochrome *c* expressed in *Escherichia coli*, *Protein Expression Purif. 22*, 220−224.
18. Satoh, T., Itoga, A., Isogai, Y., Kurihara, M., Yamada, S., Natori, M., Suzuki, N., Suruga, K., Kawachi, R., Arahira, M., Nishio, T., Fukazawa, C., and Oku, T. (2002) Increasing the conformational stability by replacement of heme axial ligand in *c*-type cytochrome, *FEBS Lett. 531*, 543−547.
19. Barker, P. D., Ferrer, J. C., Mylrajan, M., Loehr, T. M., Feng, R., Konishi, Y., Funk, W. D., MacGillivray, R. T., and Mauk, A. G. (1993) Transmutation of a heme protein, *Proc. Natl. Acad. Sci. U.S.A. 90*, 6542−6546.
20. Barker, P. D., Nerou, E. P., Freund, S. M., and Fearnley, I. M. (1995) Conversion of cytochrome b_{562} to *c*-type cytochromes, *Biochemistry 34*, 15191−15203.
21. Daltrop, O., Allen, J. W. A., Willis, A. C., and Ferguson, S. J. (2002) *In vitro* formation of a *c*-type cytochrome, *Proc. Natl. Acad. Sci. U.S.A. 99*, 7872−7876.
22. Daltrop, O., and Ferguson, S. J. (2003) Cytochrome *c* maturation. The *in vitro* reactions of horse heart apocytochrome *c* and *Paracoccus denitrificans* apocytochrome c_{550} with heme, *J. Biol. Chem. 278*, 4404−4409.
23. Sharp, P. M., Cowe, E., Higgins, D. G., Shields, D. C., Wolfe, K. H., and Wright, F. (1988) Codon usage patterns in *Escherichia coli*, *Bacillus subtilis*, *Saccharomyces cerevisiae*, *Schizosaccharomyces pombe*, *Drosophila melanogaster* and *Homo sapiens*; a review of the considerable within-species diversity, *Nucleic Acids Res. 16*, 8207−8211.
24. Pettigrew, G. W., Leaver, J. L., Meyer, T. E., and Ryle, A. P. (1975) Purification, properties and amino acid sequence of atypical cytochrome *c* from two Protozoa, *Euglena gracilis* and *Crithidia oncopelti*, *Biochem. J. 147*, 291−302.
25. Suckau, D., Resemann, A., Schuerenberg, M., Hufnagel, P., Franzen, J., and Holle, A. (2003) A novel MALDI LIFT-TOF/TOF mass spectrometer for proteomics, *Anal. Bioanal. Chem. 376*, 952−965.
26. Dutton, P. L. (1978) Redox potentiometry: determination of midpoint potentials of oxidation−reduction components of biological electron-transfer systems, *Methods Enzymol. 54*, 411−435.
27. Masaki, T., Tanabe, M., Nakamura, K., and Soejima, M. (1981) Studies on a new proteolytic enzyme from *Achromobacter lyticus* M497-1. I. Purification and some enzymatic properties, *Biochim. Biophys. Acta 660*, 44−50.
28. Pace, C. N., Shirley, B. A., and Thompson, J. A. (1989) in *Protein structure: A Practical Approach* (Creighton, T. E., Ed.) pp 311−330, IRL, Oxford, U.K.
29. Tomlinson, E. J., and Ferguson, S. J. (2000) Conversion of a *c* type cytochrome to a *b* type that spontaneously forms *in vitro* from apo protein and heme: implications for *c* type cytochrome biogenesis and folding, *Proc. Natl. Acad. Sci. U.S.A. 97*, 5156−5160.
30. Tomlinson, E. J., and Ferguson, S. J. (2000) Loss of either of the two heme-binding cysteines from a class I *c*-type cytochrome has a surprisingly small effect on physicochemical properties, *J. Biol. Chem. 275*, 32530−32534.
31. von Bodman, S. B., Schuler, M. A., Jollie, D. R., and Sligar, S. G. (1986) Synthesis, bacterial expression, and mutagenesis of the gene coding for mammalian cytochrome b_5, *Proc. Natl. Acad. Sci. U.S.A. 83*, 9443−9447.
32. Barker, P. D., Nerou, E. P., Cheesman, M. R., Thomson, A. J., de Oliveira, P., and Hill, H. A. O. (1996) Bis-methionine ligation to heme iron in mutants of cytochrome b_{562}. 1. Spectroscopic and electrochemical characterization of the electronic properties, *Biochemistry 35*, 13618−13626.
33. Allen, J. W. A., Barker, P. D., and Ferguson, S. J. (2003) A cytochrome b_{562} variant with a *c*-type cytochrome CXXCH heme-binding motif as a probe of the *Escherichia coli* cytochrome *c* maturation system, *J. Biol. Chem. 278*, 52075−52083.
34. Daltrop, O., Smith, K. M., and Ferguson, S. J. (2003) Stereoselective *in vitro* formation of *c*-type cytochrome variants from *Hydrogenobacter thermophilus* containing only a single thioether bond, *J. Biol. Chem. 278*, 24308−24313.
35. Keightley, J. A., Sanders, D., Todaro, T. R., Pastuszyn, A., and Fee, J. A. (1998) Cloning and expression in *Escherichia coli* of the cytochrome c_{552} gene from *Thermus thermophilus* HB8, *J. Biol. Chem. 273*, 12006−12016.
36. McRee, D. E., Williams, P. A., Sridhar, V., Pastuszyn, A., Bren, K. L., Patel, K. M., Chen, Y., Todaro, T. R., Sanders, D., Luna, E., and Fee, J. A. (2001) Recombinant cytochrome rC_{557} obtained from *Escherichia coli* cells expressing a truncated *Thermus thermophilus cyc*A gene. Heme inversion in an improperly matured protein, *J. Biol. Chem. 276*, 537−544.
37. Raphael, A. L., and Gray, H. B. (1989) Axial ligand replacement in horse heart cytochrome *c* by semisynthesis, *Proteins: Struct., Funct., Genet. 6*, 338−340.
38. Rosell, F. I., and Mauk, A. G. (2002) Spectroscopic properties of a mitochondrial cytochrome *c* with a single thioether bond to the heme prosthetic group, *Biochemistry 41*, 7811−7818.
39. Pollock, W. B. R., Rosell, F. I., Twitchett, M. B., Dumont, M. E., and Mauk, A. G. (1998) Bacterial expression of a mitochondrial cytochrome *c*. Trimethylation of Lys72 in yeast iso-1-cytochrome *c* and the alkaline conformational transition, *Biochemistry 37*, 6124−6131.

40. Gibney, B. R., Isogai, Y., Rabanal, F., Reddy, K. S., Grosset, A. M., Moser, C. C., and Dutton, P. L. (2000) Self-assembly of heme A and heme B in a designed four-helix bundle: implications for a cytochrome *c* oxidase maquette, *Biochemistry 39*, 11041−11049.
41. Dill, K. A., Bromberg, S., Yue, K., Fiebig, K. M., Yee, D. P., Thomas, P. D., and Chan, H. S. (1995) Principles of protein folding: a perspective from simple exact models, *Protein Sci. 4*, 561−602.
42. Hill, R. B., and DeGrado, W. F. (1998) Solution structure of α_2D, a nativelike de novo designed protein, *J. Am. Chem. Soc. 120*, 1138−1145.
43. Shifman, J. M., Gibney, B. R., Sharp, R. E., and Dutton, P. L. (2000) Heme redox potential control in *de novo* designed four-α-helix bundle proteins, *Biochemistry 39*, 14813−14821.
44. Gibney, B. R., Huang, S. S., Skalicky, J. J., Fuentes, E. J., Wand, A. J., and Dutton, P. L. (2001) Hydrophobic modulation of heme properties in heme protein maquettes, *Biochemistry 40*, 10550−10561.
45. Grosset, A. M., Gibney, B. R., Rabanal, F., Moser, C. C., and Dutton, P. L. (2001) Proof of principle in a de novo designed protein maquette: An allosterically regulated, charge-activated conformational switch in a tetra-α-helix bundle, *Biochemistry 40*, 5474−5487.
46. Bard, A. J., and Faulkner, L. R. (2001) in *Electrochemical methods: fundamentals and applications*, 2nd ed., Wiley, New York.
47. Xu, Z. J., and Farid, R. S. (2001) Design, synthesis, and characterization of a novel hemoprotein, *Protein Sci. 10*, 236−249.
48. Huang, S. S., Gibney, B. R., Stayrook, S. E., Dutton, P. L., and Lewis, M. (2003) X-ray structure of a maquette scaffold, *J. Mol. Biol. 326*, 1219−1225.
49. Gunner, M. R., and Honig, B. (1991) Electrostatic control of midpoint potentials in the cytochrome subunit of the *Rhodopseudomonas viridis* reaction center, *Proc. Natl. Acad. Sci. U.S.A. 88*, 9151−9155.
50. Skalicky, J. J., Gibney, B. R., Rabanal, F., Bieber, U. R. J., Dutton, P. L., and Wand, A. J. (1999) Solution structure of a designed four-α-helix bundle maquette scaffold, *J. Am. Chem. Soc. 121*, 4941−4951.
51. McGuirl, M. A., Lee, J. C., Lyubovitsky, J. G., Thanyakoop, C., Richards, J. H., Gray, H. B., and Winkler, J. R. (2003) Cloning, heterologous expression, and characterization of recombinant class II cytochromes *c* from *Rhodopseudomonas palustris*, *Biochim. Biophys. Acta 1619*, 23−28.

BI049546E